crystals

MDPI

Article

Investigation of the Grain Boundary Character and Dislocation Density of Different Types of High Performance Multicrystalline Silicon

Gaute Stokkan [1,*], Adolphus Song [2] and Birgit Ryningen [1]

[1] Solar Cell Silicon Group, Department of Sustainable Energy Technology, SINTEF Industry, P.O. Box 4760 Torgarden, 7465 Trondheim, Norway; birgit.ryningen@sintef.no

[2] REC Solar Pte. Ltd., 20 Tuas South Ave. 14, Singapore 637312, Singapore; adolphus.song@recgroup.com

* Correspondence: gaute.stokkan@sintef.no; Tel.: +47-415-59851

Received: 18 July 2018; Accepted: 21 August 2018; Published: 24 August 2018

Abstract: Wafers from three heights and two different lateral positions (corner and centre) of four industrial multicrystalline silicon ingots were analysed with respect to their grain structure and dislocation density. Three of the ingots were non-seeded and one ingot was seeded. It was found that there is a strong correlation between the ratio of the densities of (coincidence site lattice) CSL grain boundaries and high angle grain boundaries in the bottom of a block and the dislocation cluster density higher in the block. In general, the seeded blocks, both the corner and centre block, have a lower dislocation cluster density than in the non-seeded blocks, which displayed a large variation. The density of the random angle boundaries in the corner blocks of the non-seeded ingots was similar to the density in the seeded ingots, while the density in the centre blocks was lower. However, the density of CSL boundaries was higher in all the non-seeded than in the seeded ingots. It appears that both of these grain boundary densities influence the presence of dislocation clusters, and we propose they act as dislocation sinks and sources, respectively. The ability to generate small grain size material without seeding appears to be correlated to the morphology of the coating, which is generally rougher in the corner positions than in the middle. Furthermore, the density of twins and CSL boundaries depends on the growth mode during initial growth and thus on the degree of supercooling. Controlling both these properties is important in order to be able to successfully produce uniform quality high-performance multicrystalline silicon by the advantageous non-seeding method.

Keywords: silicon; crystallisation; dislocation density; defect; grain boundaries

1. Introduction

Multicrystalline silicon is the dominant material for solar cell production, and its fraction of the total production volume is increasing, accounting for 62.4% in 2017 [1]. Its strong position is a consequence of its relatively simple production process compared to the alternatives and its relatively high achievable efficiency. The increasing trend in dominance, despite the fact that multicrystalline silicon cannot be used in the very-high-efficiency cell architectures and thus demands more balance of system costs, may be a result of its very good process scalability. Processes for large ingot production have been readily developed. In addition, the material quality has been quite radically improved during the last few years. The material quality that has taken over the market is termed high-performance multicrystalline silicon (HPMC-Si) and has the following characteristics [2,3]:

- Dislocation clusters are far less abundant than in conventional material, and the clusters do not proliferate uncontrollably as growth proceeds (i.e., upwards in the ingot);

- Grain sizes are smaller than before, starting in the mm^2 size, growing to cm^2 towards the top. Previously, very large grains developed even at the very bottom of the ingot without grain selection, and several cm^2 would be expected at the top;
- Grain boundaries have a different structure and composition than before; whereas the large majority of grain boundaries used to be coincidence site lattice (CSL) boundaries, particularly of the Σ3 type, currently a much larger proportion of random angle grain boundaries (RAGB) is present.

The decreased occurrence of dislocation clusters is the explanation for the improved quality. This decreased occurrence is linked to the small grain size and the different grain boundary configuration; however, the mechanisms that link the phenomena are not understood.

It is known that dislocation clusters can be traced downwards in the ingot while decreasing in size, and the first point of observation is primarily at a grain boundary [4–6]. These boundaries are almost exclusively CSL boundaries, and Σ27 boundaries have been observed in high proportions [4,5,7] while other boundaries are also seen [5], although never of the RAGB type. CSL boundaries are generally low energy configurations since atoms in the two corresponding lattices of the two grains share a certain proportion of common lattice sites, particularly when the boundaries adhere to low energy planes [8]. However, in macroscopic crystals, the boundaries do not necessarily follow these planes, and intricate structures including grain boundary splitting and faceting are observed when such deviation occurs [9]. Observations indicate that dislocation emission occurs predominantly at such structures [10], and it is believed that the kinks/steps/facets act as stress concentrators, which lower the barrier for dislocation nucleation. The Σ27 boundary is not a particularly low energy boundary [8], and such deviation from low energy plane configurations may therefore be expected to happen relatively often, making this boundary type a particularly potent source considering its relatively frequent occurrence. One possible explanation for the decreased occurrence of dislocation clusters may therefore be that this material contains a decreased density of generation sites.

It has, however, been observed [2] that dislocation clusters do tend to appear but do not proliferate laterally, and they also have a limited vertical extension; i.e., if we consider these dislocation clusters to be a growth phenomenon, they are terminated after a while. Stokkan et al. studied the emergence and disappearance of dislocation clusters, the relationship between cluster height and lateral extension, and the conditions as dislocation clusters which disappeared in HPMC-Si [11]. It was shown that a large lateral and vertical extension correlated very well; i.e., if the dislocation clusters are allowed to grow tall, they will also be wide, and vice versa. Secondly, the tall and wide clusters became increasingly common towards the top, which correlates with an increasing grain size. Finally, it was shown that places where dislocation clusters terminated were related to interaction with a RAGB; i.e., the dislocated grain was overgrown by another grain with fewer dislocations, and the individual dislocations terminated at RAGB boundaries between the grains. It was proposed that the limited proliferation and lower density of dislocation clusters was caused by such overgrowth, and the decreased dislocation cluster density could be the result of an increased density of "dislocation sinks".

A third possible explanation is that the higher proportion of RAGBs lead to the release of global thermal stress at these boundaries [3] rather than the concentration of stress at CSL boundaries. This would cause less dislocation nucleation and less movement of dislocations, leading to less interaction with dislocations of different slip systems [12] and less multiplication. So far, the termination at RAGBs is the explanation which is most consistent with the observation of small clusters which are limited in height. For all the mechanisms discussed, the type and density of grain boundaries is of high importance.

It should be noted that there is no universal method of producing material with the characteristics listed as descriptive of HPMC-Si. While the most common method employed industrially is the use of a seeding layer at the crucible bottom consisting of small grained polycrystalline silicon, it is also possible to achieve the same characteristics using a charge that is initially fully melted and then nucleated on the silicon nitride powder coating which is applied on the inside of the quartz crucible to

prevent direct chemical contact and sticking between crucible and silicon. It is clear that controlling the temperature during the nucleation step as well as the properties of the coating will be very important in order to succeed using the latter method. The possible benefit of such a method is, of course, its lower requirements for controlling the melting phase accurately and a higher volume yield, since it is necessary to remove the seeding layer as well as an increased "red zone" thickness generated by the former method.

It is worth noting, and will be discussed further in this paper, that there is a fundamental difference in the initial growth phase of these two methods. While the seeding method does not require supercooling to initiate growth on the seeds, the non-seeded method requires supercooling in order for nuclei of sufficient size to develop, and this supercooling will exist also at the transition to initial growth, influencing both the speed and direction of growth, and it may also influence the growth mode, i.e., planar vs. dendritic growth [13]. We will therefore in this paper consider two different initial conditions: seeded growth and nucleated growth, corresponding to seeded and non-seeded ingots.

Considering the likely influence of coating on the nucleation properties, it is interesting to study the effect of different coating morphologies on the crystal properties. Such differences in coating morphology may be a deliberate measure, e.g., different patterns may be artificially shaped in the coating, or may be a result of the production process, e.g., different roughness may result from different drying conditions and turbulence patterns during the spraying in different parts of the crucible.

In this paper, seeded and non-seeded crystals will be investigated and compared, and also the effect of different coating properties will be investigated. The metrics used are related to the characteristics mentioned initially: the dislocation density or density of dislocation clusters, and the grain size, density and composition of grain boundaries of different types. As will be seen, the latter two will be related, since it is necessary to define a method of measuring grain size, and this method will necessarily be governed by which grain boundary types are considered.

2. Materials and Methods

Wafers from three heights and two different lateral positions (corner and centre) of four industrial ingots were analysed with respect to their grain structure and dislocation density. These ingots were produced by REC Solar at their factory in Singapore in 2014 and are thus not representative of current production. Three of the ingots were non-seeded and one ingot was seeded. The HPMC-Si properties of the non-seeded ingots were obtained by controlling the temperature time and space gradients during nucleation and initial growth, details of which are not disclosed. However, they were representative of the standard production at the time, and the basic properties of the process remain the same in current production. The non-seeded ingots had a 20 mm thick part removed from the bottom prior to wafering. This is common procedure for industrial material to remove the severely contaminated part which is unsuitable for cell processing, the red-zone. The seeded blocks had an even thicker part removed due to remaining unmelted material and a thicker red-zone. It is not known how far above the unmelted seed material the wafering started. The wafers were taken from bottom, middle and top positions, i.e., wafers 1, 300 and 400 in the seeded and 1, 300 and 600 in the non-seeded ingots. In total, 24 wafers were analysed. The wafers were 180 μm thick, and the thickness removed in the cutting was 141 μm, which corresponds to a total height of 193mm for a 600-wafer stack.

Two of the non-seeded ingots were produced with regular silicon nitride coating made in-house, while the third was produced using a slightly rougher coating aimed at promoting random nucleation. This ingot was furthermore of size G4 (4×4 blocks of lateral area 156×156 mm^2) while the other ingots in the study were G5 (5×5 blocks). An overview of the ingot properties is given in Table 1.

From the 156×156 mm^2 wafers, nine 50×50 mm^2 samples were cut by laser scribing, and one of these was polished to a mirror finish and analysed by electron back scatter diffraction (EBSD). The same area was analysed for all 156×156 mm^2 wafers. The EBSD measurements were performed using a JEOL JSM 840A Scanning Electron Microscope equipped with TSL OIM software for data acquisition and analysis and a NORDIF Phosphor detector. In order to obtain large-scale measurements

for statistical analysis, the Comboscan mode was used, in which several areas are imaged by scanning the electron beam, with each scan separated by a transfer of the sample stage. The acquisition software stitches these images together to form a large area measurement. The stage movement is time consuming, and therefore it is time efficient to perform as few transfers as possible, and a very low magnification of 30× is used despite the fact that this results in image distortion. The images are still of sufficient quality for statistical purposes. The beam step size was 100 µm. An area of ~30 × 40 mm^2 was scanned for all the wafers.

Table 1. Overview of ingot properties.

Ingot Label	Initial Growth	Size	Coating
VH1	non-seeded	G5	regular
VH2	non-seeded	G5	regular
G4VHP	non-seeded	G4	enhanced roughness
MS/multiseed	seeded	G5	not relevant

The wafers were thereafter etched in Sopori etch [14] to reveal dislocations as etch pits and grain boundaries as grooves. The etch pit density was counted by PVScan [15], a tool that provides quantified measurements of dislocation density based on the detection of diffusely scattered light from the etch pits. A calibration routine based on a combination of two curve fitting models provides realistic numbers in both high-density (~10^6 cm^{-2}) and low -ensity (~10^4 cm^{-2}) regions. Highly twinned regions will result in a strong signal, which is erroneously interpreted as a high dislocation density [16], which must be manually corrected. The measurement resolution was 200 µm. In order to be able to manually correct for erroneously interpreted twins, the area fraction of dislocation clusters was obtained by image analysis of the RGB density plots using the colour range selection functionality in Adobe Photoshop software (version CS5 Extended, 12.1 × 64). All areas corresponding to low density were selected by sampling an area of very low etch pit density and setting an appropriate "fuzziness" that expands the colour range selection. This ranges from 0 (very small area selected) to 200 (very large area selected), and a setting of 150 resulted in the selection of all areas below the density of ~1 × 10^6 cm^{-2}. The cluster area was determined by simply inverting the selection. Clearly twinned regions could easily be manually deselected, and the procedure proved superior to other automated methods, provided the chosen metric is, as here, the area density of dislocation clusters with an etch pit density above ~1 × 10^6 cm^{-2}.

Since it is not possible to perform measurements on the actual crucibles used in the crystallization process, coating morphology was measured on samples taken from crucibles that were coated by the same method as ingots VH1/VH2 and G4VHP, respectively, by the use of a confocal microscope at 5 and 20× magnification. The coating method is fully automated, and we expect the morphology measured to be representative of the coating used to make the ingots. After coating the crucibles by the normal procedure, the crucibles were crushed, and samples were selected from the corner and centre positions for roughness analysis.

3. Results

3.1. Grain Size

A visual impression of the grain size can be obtained from orientation image maps (OIM), or from individual grain images (IGI), where all individual grains are coloured with a unique colour, independent of the crystal orientation. Orientation image maps of the bottom, middle and top wafers of a corner block from one of the reference non-seeded ingots are shown in the top row of Figure 1. The left column shows IGIs of the bottom wafer of the same block and two other blocks: the centre block of the same ingot and a corner block of a seeded ingot (the behaviour of centre and corner blocks in the seeded ingots are very similar, and the centre block is not shown). In these IGIs, all crystals

of different orientation are defined as grains. The visual impression of the OIM and the IGI of the different bottom wafers is very similar. However, the purpose of this study is to investigate the effect of different conditions during nucleation and initial growth on defect properties, and it makes sense to discard all information about twinning. This is justified since twins generally do not influence the recombination of carriers, and we furthermore suppose that twins separate grains of common origin: either these are remaining twins from initial dendritic growth, or they result from the frequently observed growth twinning occurring inside one grain, generally initiated at the grain boundaries [17]. IGIs were made where twins were disregarded, and examples of these for the mentioned blocks and positions constitute the rest of Figure 1. Some observations can be made:

- The IGIs where twins are included indicate that the bottom wafers of the non-seeded ingot have an overall smaller grain size than the seeded ingot;
- This relation is reversed when twins are disregarded. This is particularly evident for the centre block;
- Further up in the ingot, the difference between seeded and non-seeded decreases; however, the grain size in the centre block is generally somewhat larger.

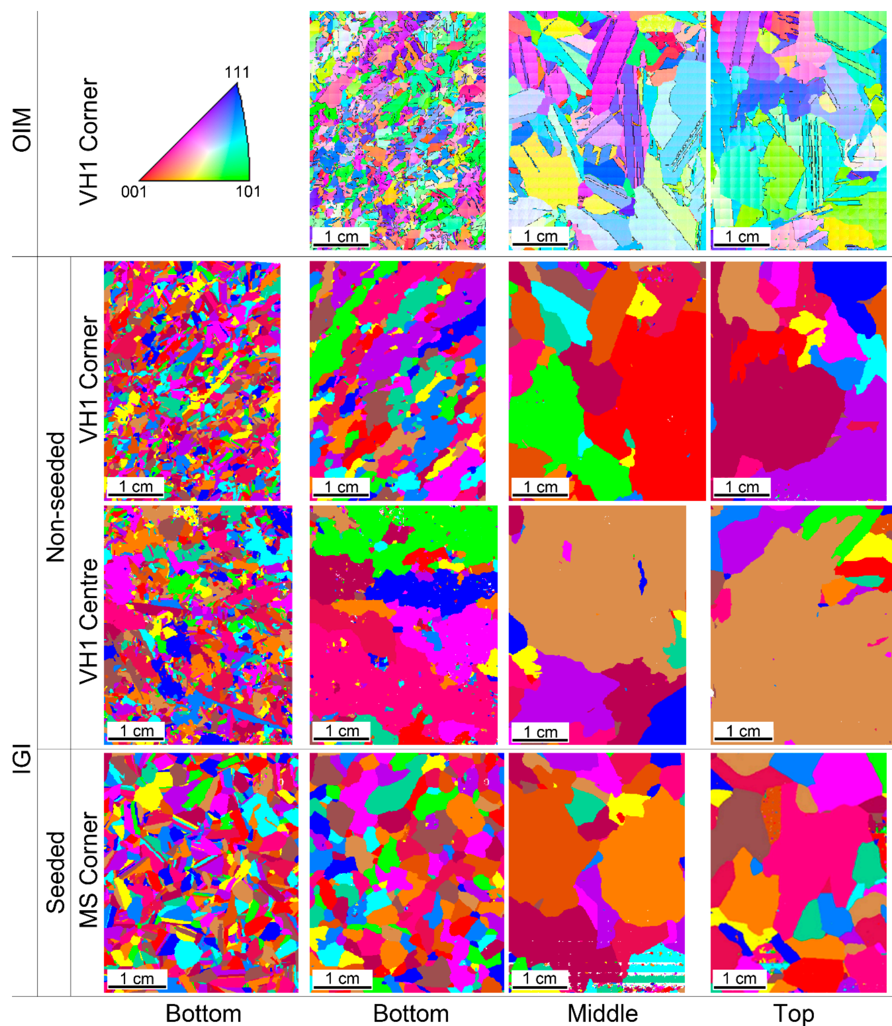

Figure 1. Orientation image micrographs (OIM) and individual grain images (IGI) of selected samples: Bottom, middle and top positions of corner and centre blocks from one of the reference non-seeded ingots (VH1) and corner block from a seeded ingot. IGIs include twin boundaries in the leftmost column but disregard these in the three other columns. The bottom, middle and top positions refer to wafer number 1, 300 and 600 for non-seeded ingots and 1, 300 and 400 for seeded ingots, respectively.

A quantification of the grain size compatible with the IGIs in Figure 1 is simply the total density of boundaries without a $\Sigma3^n$ relation, since the EBSD analysis software disregards boundaries with a misorientation below 5°; i.e., the vast majority of sub-grain boundaries in silicon. Since other CSL boundaries such as Σ5, Σ11 etc. exist in a very small density compared to the $\Sigma3^n$ (e.g., [18]), this number roughly corresponds to the total density of random angle grain boundaries (RAGB). This parameter is given in Figure 2a as a function of block height for all the samples investigated. The indications above are confirmed; corner non-seeded blocks and seeded blocks (regardless of position) form one group while centre non-seeded blocks form a different group with larger grains than the first. Furthermore, the following trends can be seen: for all the blocks in this study, the grain size increases with height. Thus increase in grain size is significantly higher from the bottom to the middle of the ingots compared to from the middle to top of the ingot. In general, the density of random angle grain boundaries is halved from the bottom to the middle of the ingot. From middle to top, there is either a very small or negligible increase in grain size, or in some cases a decrease. Notably, although the grain size appears to stabilize from the middle of the ingot and upwards, there is still a noticeable difference in the top, indicating that, for this material, an effect of the small grain size achieved for corner non-seeded blocks and seeded blocks still influences the properties towards the top.

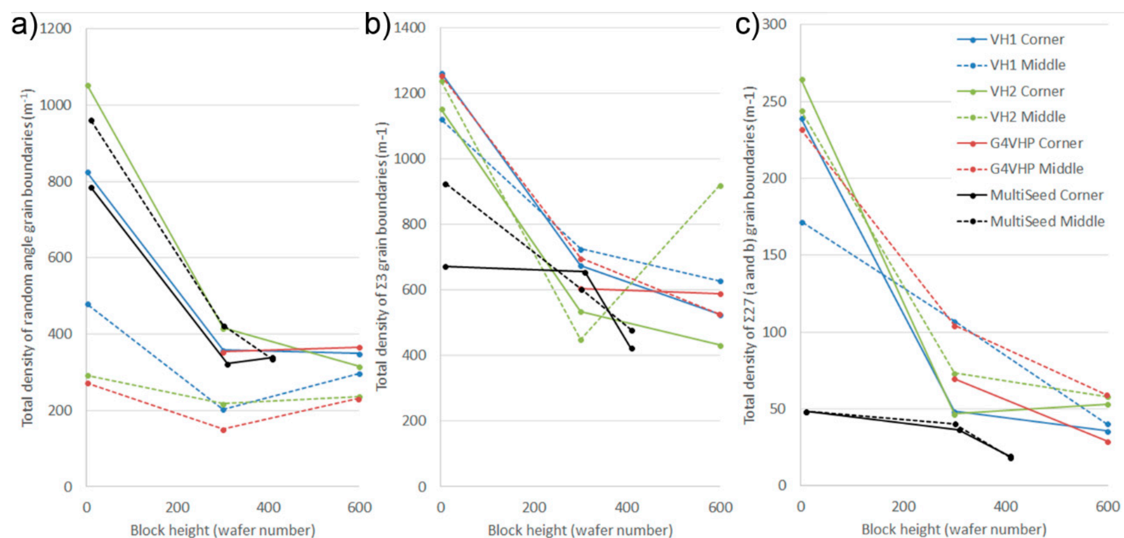

Figure 2. (**a**) Total density of random angle grain boundaries vs. block height (the numbers may contain a very small fraction of non $\Sigma3^n$ boundaries, which however are so uncommon in silicon such as not to disturb the general trend. Sub grain boundaries with misorientation <5° are not included; (**b**) The total density of Σ3 boundaries vs. block height; (**c**) The total density of Σ27 (**a**,**b**) grain boundaries vs. wafer number.

3.2. Grain Boundaries

Figure 2b shows the density of Σ3 boundaries in a similar graph as Figure 2a. For all the blocks except one, the total density of Σ3 grain boundaries decreases with height. The top wafer in the block with deviating behaviour (green, dashed line) is dominated by a few grains with profound multiple twinning. The twin density in the bottom wafers is somewhat higher in the non-seeded than in the seeded wafers, but there is no noticeable difference between the corner and centre blocks of the non-seeded blocks.

The density of third-order twins, i.e., Σ27 boundaries (Figure 2c), shows a similar trend as first-order twins, but the difference between seeded and non-seeded is quite a bit more distinct. There is no clear trend comparing corner and middle positions in the bottom, but the density becomes somewhat smaller in the corner blocks than the centre blocks towards the middle and top positions.

Standard ingots of traditional multicrystalline silicon are reported to have a length fraction of Σ3 of about 80% [18] and a random angle grain boundary fraction of less than 10%. As can be seen in Figure 3, with the exception of the upper part of one of the non-seeded centre blocks, all the ingots in this study had a length fraction of Σ3 boundaries of between 40 and 60%. The fraction of RAGBs varies between 10 and 40% and is smallest in the middle non-seeded blocks and highest in the seeded and corner non-seeded blocks.

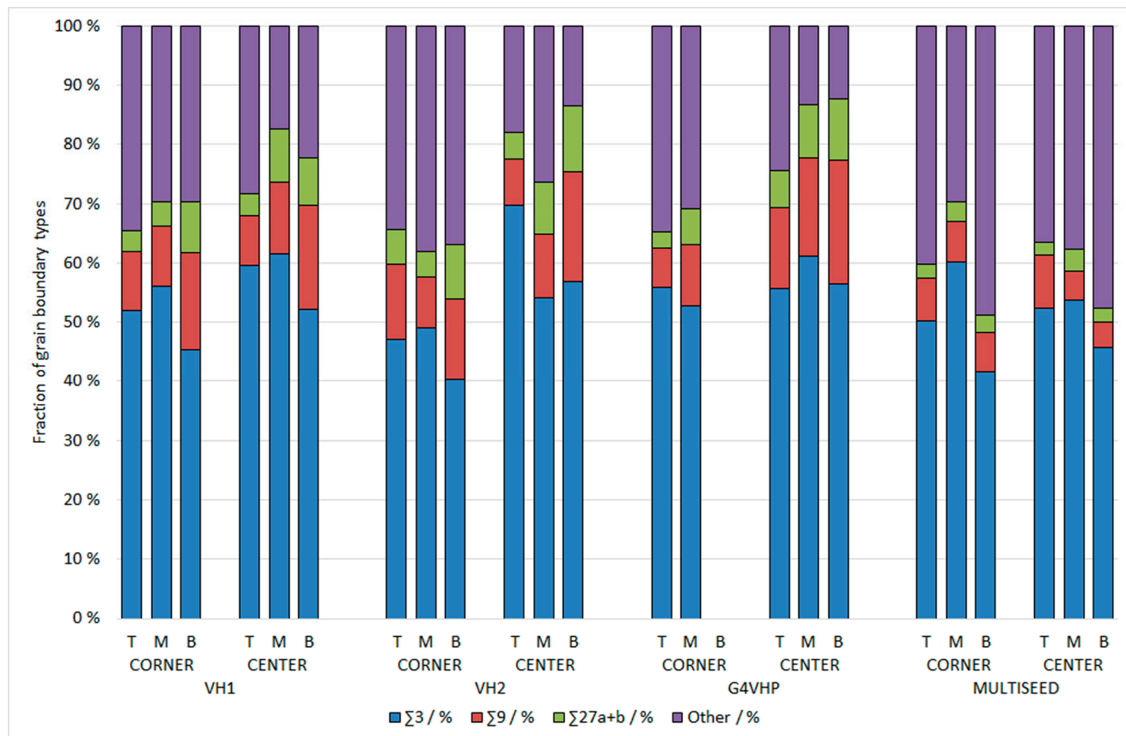

Figure 3. Fraction of different grain boundary types for the samples in the study.

3.3. Dislocation Density

Dislocation densities measured by PVScan for the same set of wafers that are shown in Figure 1 are given in Figure 4a, and the density of the dislocation clusters determined according to the procedure described in the experimental section is shown in Figure 4b. The samples form three groups: (1) the seeded ingots have the lowest dislocation cluster density; (2) the non-seeded corner blocks have a medium density; and (3) the non-seeded centre blocks have the highest density throughout the height. One of the centre blocks appears to be slightly better than the two others. The non-seeded ingots generally show an increasing trend towards the top, while this is not so clear for the seeded ingot. However, it should be noted that the grain boundary artefact on dislocation density measurements by PVScan is more pronounced in the bottom wafers, and the apparently higher dislocation cluster density in the middle-bottom seeded wafer may be due to this.

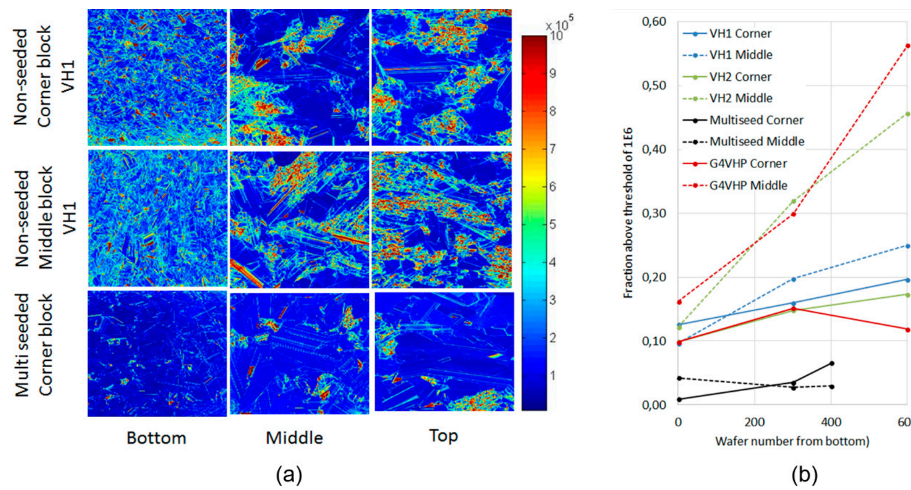

Figure 4. (**a**) Dislocation density maps of wafer number 001, 301 and 601 of a corner and centre block of a non-seeded ingot (VH1) and the dislocation density maps of wafers 009, 309 and 409 from a corner block of the seeded ingot; (**b**) Density of dislocation clusters as function of height in ingot.

3.4. Coating Morphology

Examples of the coating morphology measurements are shown in Figure 5. Numerical results are given in Table 2. There is a marked difference between centre and corner positions for both crucible types on both measurement scales. There are no significant differences between the coating types (VH1/VH2 vs. G4VHP) for the arithmetic average roughness, R_a, which is a measure of average vertical roughness, but the mean spacing of profile irregularities, S_m, which measures lateral variations, indicates that G4VHP has variations on a larger scale than VH1/VH2.

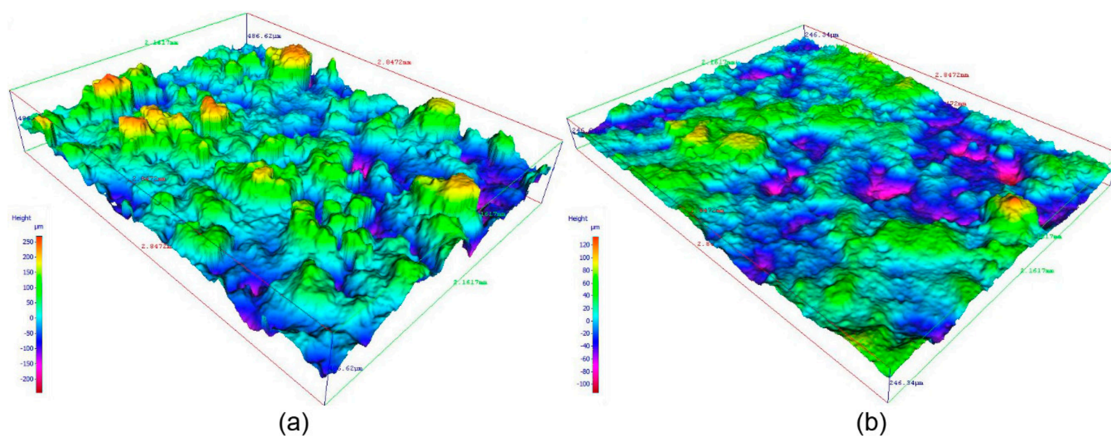

Figure 5. Measurements of coating morphology using confocal microscope at 5× magnification. (**a**) Corner sample; (**b**) centre sample.

Table 2. Surface roughness parameters for coating. Average roughness, R_a, is reported for 5× and 20× magnification while mean spacing of profile irregularities, S_m is reported for 5× magnification only.

	Similar to G4VHP		**Similar to VH1/VH2**	
5×	corner	center	corner	center
R_a (μm)	13.96	8.35	15.46	5.15
S_m (μm)	408.58	403.46	288.62	241.56
20×	corner	center	corner	center
R_a(μm)	5.36	1.64	5.42	2.27

4. Discussion

4.1. Mechanisms Controlling Grain Boundary Density

Our study aims to investigate how nucleation and seeding influences the generation of grain boundaries and dislocations. It is important to select suitable metrics to elucidate such relations. In our opinion, the percentage distribution of grain boundary types (as shown in Figure 3) is not very suited for this, although it is often used and reported. The density of grain boundaries (Figure 2) is more suitable because it is an absolute value that can be related to a physical phenomenon. We have argued that the total random angle grain boundary density is a measure of grain size that reflects how crystals with different orientation still pertain to the same origin through growth twinning or twinned dendrites during initial growth. Equivalently, the density of $\Sigma 3$ and $\Sigma 3^n$ boundaries reflect how important these two phenomena are. Furthermore, if the starting conditions are similar for two different positions (or ingots, provided the growth conditions are similar), there is no reason to believe that the amount of growth twinning should be different. Therefore, any observable difference in the density of these grain boundaries can also likely be assumed to relate to the initial growth conditions, but the physical mechanism causing variations in twin density may be different than for the random angle boundaries. We will show how the analysis of these data sets together with dislocation measurements show which mechanisms are important.

For dislocations, we chose the density of clusters as metric because the presence of such clusters relates directly to the generation [4] or disappearance [11] of dislocations at grain boundaries, i.e., those mechanisms mainly related to grain boundaries, while the average dislocation density or dislocation density distribution can be assumed to depend also heavily on multiplication [12].

The random angle grain boundary densities in Figure 2 form two groups: corner non-seeded blocks and seeded blocks (higher density) in one group and centre blocks (lower density) in the other group. The fact that the seeded ingots present very little difference between the lateral positions indicates that the difference is caused by factors related to nucleation or very early growth. It appears possible to achieve the same grain size by both a nucleation mechanism and by growth on seeds. It is, however, difficult to achieve high density uniformly by nucleation. The difference between corner and middle may be related to different thermal conditions in the two regions, which may also lead to differences in thermal stress, or to different conditions for heterogeneous nucleation, i.e., differences in the coating/melt interface. Although we do not know the thermal conditions at the crucible bottom in detail, we believe the latter explanation is more likely since the nucleation of small grains require a careful control of the change of the thermal field in the bottom during this phase, which is unlikely to change much between the time when the middle and the corner is nucleated. Furthermore, the difference in coating morphology between the middle and the corner is quite striking. Since the coating is not wetted by the molten silicon, the contact between the coating and the melt is limited to certain points, while the melt is suspended between these [13]. The density and condition of nucleation sites is therefore very likely to correlate with the morphology of the coating. We therefore propose that in the non-seeded method, the actual grain size can be controlled mainly by controlling the morphology of the coating, and that roughness differences on a vertical scale of 10 µm are an important factor here. The importance of coating roughness on the nucleation has been pointed out earlier. A roughness difference in the same order of magnitude produced two ingots with pronounced different crystallography in a pilot-scale Bridgeman furnace. The ingot produced with the rougher coating had large grains due to dendritic nucleation in the bottom, whereas the ingot produced with a slightly smoother coating layer had small grains with more random orientations [19]. This is the opposite behaviour to what is reported here and illustrates the challenges connected to the non-seeded approach and the small temperature gradient window available, as pointed out already by Yang [2]. Note that the measured grain size is in the range of mm, whereas the lateral roughness is on a scale of 100 µm, i.e., a factor 100 difference. Thus, only a few of the nucleation sites induced by the coating-melt contact have actually resulted in grains being present at this height (~20 mm above the bottom),

i.e., either significant grain growth has occurred or only a few nuclei proceed into the initial growth phase. Observations of generally large grains in bottom slabs indicate that the latter is the most likely explanation.

We see in Figure 1 that the difference between the apparent grain structure and the actual grain structure in the bottom when twins are disregarded is only slight for the seeded ingot, while it is clear for the non-seeded corner samples and striking for the non-seeded middle samples. The latter two also have a prolonged grain shape; most notable is the diagonal pattern in the corner sample. This is probably related to lateral temperature gradients along the crucible bottom and a preferred growth along this gradient. Figure 3 shows that there is no difference in the twin density between corner and middle non-seeded blocks, and so it is only the different density of random angle grain boundaries that determines the difference between the positions in the same ingot. Again, the blocks form two groups, which are however not the same as discussed above for random angle boundary density: here, the non-seeded blocks have a higher twin density than the seeded blocks, particularly in the bottom. Figure 4 shows that the same grouping exists for Σ27 boundaries, and here this is even more striking: the seeded ingots have a much lower density of Σ27 than the non-seeded, which remains throughout the height. The main difference between the samples from the different groups is that one requires a nucleation phase prior to initial growth, while the second does not, and the nucleation requires a supercooling. Several groups have measured the supercooling of silicon melt on silicon nitride powder coating before nucleation [20–22], and the results vary between 0 and 40 K. However, it has been shown that the α-silicon nitride polymorph of which this coating is predominantly made is transformed to β-polymorph upon contact with silicon melt, which is accompanied by an increase in particle size [13,22]. The more recent of the studies which account for this reaction report a supercooling in the range of 0 to 10 K. The minimum supercooling required to initiate faceted dendritic growth in a silicon melt is was reported by Fujiwara et al. to be 10 K [23]. This is in the same magnitude as the supercooling numbers reported above, although in the high level of the range. However, considering differences in the experimental set-up between different studies, we think it is likely that the initial growth in the nucleated crystals is dendritic. This will explain the higher concentration of twins as well as Σ27 through branching of the dendrites. In conclusion, to control the density of twins and CSL boundaries in the non-seeded method, coating morphology is of no consequence; here, the supercooling has to be reduced by means of controlling the structure and size of the particles on which nucleation occurs, as described in the works of Ekstrøm [13] and Undheim [22,24]. It is interesting to see that this conclusion is corroborated by the observation of Brynjulfsen that coating parameters, including roughness, did not influence the supercooling [21].

4.2. Relationship between Grain Boundaries and Dislocations

We continue by investigating the possible relationship between identified grain boundary parameters and the measured dislocation cluster density. The grain boundary parameters as well as the dislocation cluster density span a large range due to the different conditions of the different ingots and positions. Therefore, we attempted to fit the different grain boundary data (from all the ingots) to the dislocation cluster density over the entire range using a linear curve fit. The objective of the investigation was to find out which parameters have the best correlation, i.e., which grain boundary properties have the highest influence on dislocation cluster density. First, each vertical position was investigated by itself. Such a local correlation will be indicative of how local grain boundary properties influence the dislocation density, i.e., through multiplication by grain boundary-induced stresses, propagation in the bulk of dislocations from local sources or the release of stresses on random grain boundaries. Next, the relationship between grain boundary properties in the bottom and the dislocation cluster density in the top was investigated. A correlation here would be indicative of a situation in which grain boundary properties throughout the ingot height are largely determined in the bottom, and the dislocation density in the top is a result of the cumulative influence of grain boundaries throughout the height. This hypothesis is inspired by the existence of vertical dislocation

clusters observed by many and linked to both the generation and annihilation [11] of dislocations by grain boundaries.

An example of the first approach is shown in Figure 6a. Here, the dislocation cluster density is plotted against the density of Σ27 boundaries for the three groups. It is seen that the data form distinct groups with a linearly increasing dependence; a larger slope for higher positions. A very similar picture exists for the dislocation density vs. density of random angle grain boundaries, except that the proportionality is negative (this figure is not shown). There is no correlation at all between twin density and dislocation cluster density. A parameter we have chosen to call source/sink, i.e., the density of Σ27 boundaries (dislocation source boundaries) divided by the density of random angle grain boundaries (dislocation sink boundaries), shows a similar trend as that seen for the Σ27 boundaries. The slopes of the linear fit curves along with the coefficients of determination (R^2) for these relations as well as those investigated below are given in Table 3.

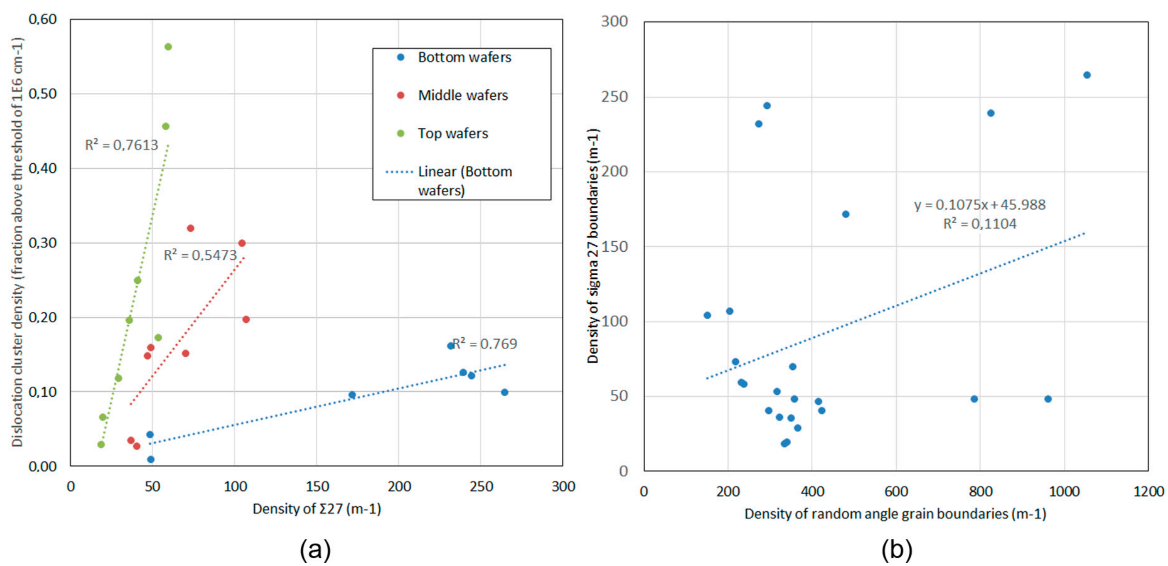

Figure 6. (**a**) Dependence of dislocation cluster density on density of Σ27 boundaries. The linear fit of bottom, middle and top wafers is shown along with the coefficient of dependence (R^2) for the three series; (**b**) Scatter plot of Σ27 (source) boundaries vs. random angle (sink) boundaries.

Table 3. Slopes and coefficients of determination for fits of grain boundary vs. dislocation cluster density data. All data have been normalized. RAGB: random angle grain boundary.

Data Series	Twins		Σ27		RAGB		Source/Sink	
	Slope	R^2	Slope	R^2	Slope	R^2	Slope	R^2
bottom wafer	0.16	0.12	0.23	0.77	−0.17	0.32	0.19	0.67
middle	−0.73	0.08	1.33	0.54	−1,5	0.60	0.53	0.55
top	1.43	0.30	4.67	0.76	−6.35	0.84	3.38	0.90
dislocations in top vs. grain boundaries in bottom	0.03	0.00	0.66	0.44	−1.0	0.76	0.88	0.98
σ27 vs. ragb	0.43	0.11						

These results can either indicate that the random angle and Σ27 boundaries both influence the dislocation cluster density or that the density of grain boundaries is interrelated (it is most likely that a high density of random angle grain boundaries leads to a low density of Σ27 boundaries). It is important to note that the numbers are actual densities, not proportions, which would imply an actual physical effect. A scatter plot of Σ27 boundary density vs. random angle boundary density is shown in Figure 6b. It is seen that there is no apparent correlation, i.e., the existence of random angle and

Σ27 boundaries appears not to be interlinked. We thus conclude that both types of grain boundaries influence the density of dislocation clusters through a physical mechanism.

However, the importance of the condition in the beginning of crystallization is demonstrated by row 4 in Table 3. While the Σ3 density in the bottom wafer shows absolutely no connection with the dislocation density in the top, both the density of Σ27 and random angle boundaries clearly correlate. The linear dependence of dislocation density on the source/sink parameter is striking and is shown in Figure 7: the higher the ratio between dislocation sources and dislocation sinks in the bottom of an ingot, the higher the dislocation cluster density will be upwards in the ingot. Apart from the different conditions during nucleation and initial growth, the ingots in this study were grown in a similar manner. Thus, the density of grain boundary types in the bottom will also define the density throughout the growth of the ingot, up until the grain growth dynamics level out such differences, which, according to Figure 2 happens around the middle and towards the top (CSL and random angle boundaries, respectively) for these ingots. The dislocation density in the top part of the ingot is the cumulative effect of actions from source and sink grain boundaries in addition to other, non-related effects such as thermal stress. Thus, in order to produce high-performance multicrystalline silicon with a low dislocation density throughout the ingot volume by the non-seeded method, it is imperative to control both the factors discussed above: the actual grain size, which appears to depend on coating morphology; and the density of the dislocation source boundaries, which depends on the initial growth mode, which in turn is determined by the size of nucleation agents and the supercooling respectively.

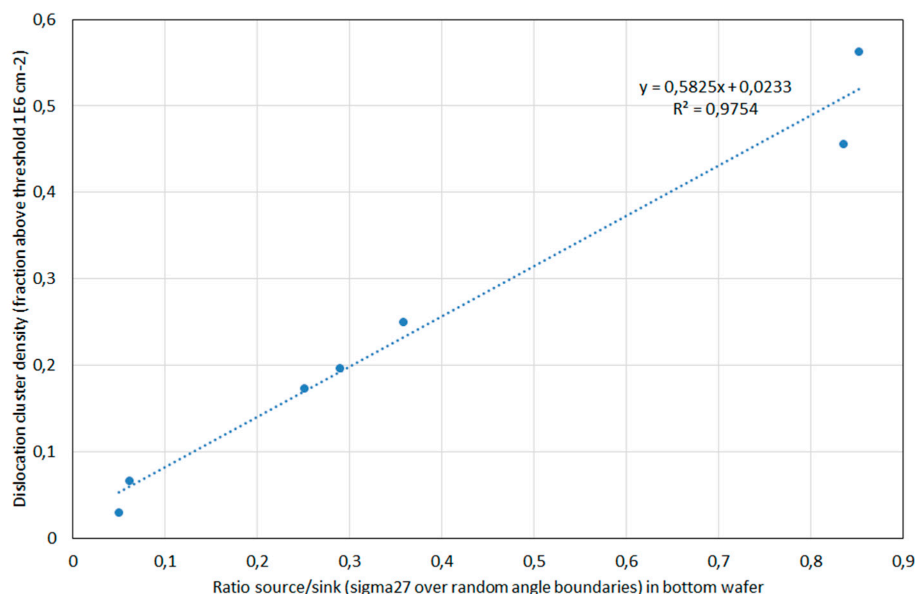

Figure 7. The ratio of dislocation "source" grain boundaries over "sink" grain boundaries in the bottom wafers versus the dislocation cluster density in the top wafers.

Since the material selection investigated in this study is restricted to one producer only, it is interesting to compare the clear trends we observe with results reported by other researchers on similar but not identical material. Investigations providing a high degree of statistics are particularly relevant for such comparison. A study by Oriwol et al. [25] investigated the evolution of dislocation clusters, noticing the different roles of different grain boundaries in blocking or transmitting dislocation propagation or even actively annihilating dislocation-rich areas. The study distinguishes between dense and light dislocation clusters, of which only the dense clusters correspond to the high density we have defined as dislocation clusters in our study. It is shown that these clusters may be actively annihilated by the migration of boundaries. These boundaries are not characterized further, but macroscopically, the shape of the grain boundary appears to be determined by features inside the

dislocated grain rather than any common low energy plane between the grains, indicating these are random angle grain boundaries. The study furthermore focuses on possible grain orientation correlation to dislocation cluster density, which we have not studied, and apart from a described mechanism where dislocations rearrange into sub grain boundaries which in turn form dislocation clusters at high temperature [26], close to the growth front (in agreement with our description), the study says little about the nature of defects acting as dislocation sources. Note that this study investigated non-HPMC-Si material only.

Lehmann et al. [27] have performed an extensive study of the development of grain orientation, grain boundary misorientation and recombination-active defects throughout the growth of multicrystalline silicon. The results are in principle possible to compare to our study since both the GB fraction of random angle grain boundaries—$\Sigma3^n$ boundaries in the bottom and top as well as the density of recombination-active defects (dislocation clusters)—are reported. Both "small grained" and "large grained" material were investigated. The results generally are in good agreement. Similar to our results, they find that differences in the density of the different grain boundary classes in the bottom wafers do not survive towards the top, where a generally stable distribution is reached (Figure 2), determined by growth kinetics. Our results indicate a possible remaining difference in the density of $\Sigma27$ boundaries when a very low density exists at the start (seeded material), which cannot be distinguished in their results since they do not report this specifically. If the ratio of the densities of $\Sigma3^n$ boundaries and random angle boundaries in the bottom are compared to the dislocation cluster density in the top, the general picture is the same as ours: a low ratio correlates to low defect density and a high ratio generally correlates to a high dislocation cluster density, while one ingot with an intermediate ratio gave an intermediate dislocation cluster density. Some discrepancy exists for the large grained material where a large ratio did not in all cases lead to a high dislocation cluster density; we note that the difference in our reporting of $\Sigma27$ boundaries and their $\Sigma3^n$ may influence this since $\Sigma27$ boundaries have a higher boundary energy than $\Sigma9$ boundaries and are thus expected to deviate from the straight, low energy structure and form steps and facets which are reported to be correlated to dislocation generation [7,10]. Also, in this study, the authors focused generally on the beneficial role of random angle grain boundaries in minimizing the area of high dislocation density, not discussing the role of dislocation sources.

Trempa et al. [28] investigated the evolution of the material parameters of conventional vs. HPMC-Si, simulating a crystallization process whereby a tall ingot of 700 mm height was grown by sequentially using the top of a regularly sized ingot as the seed for growing another regularly sized ingot. They showed that the grain boundary distribution would stabilize at a common level regardless of starting conditions above 250 mm. Nevertheless, a beneficial impact of the initial grain boundary distribution was maintained as high as 400 mm in these experiments; the results are in good agreement with ours, showing that a beneficial distribution of grain boundaries in the bottom can be seen throughout the height of regularly sized ingots.

5. Conclusions

We have shown that suitable metrics for studying the influence of nucleation and growth conditions on crystallographic properties are the total density of random angle grain boundaries, $\Sigma3$ and CSL boundaries, and the density of dislocation clusters. This allowed us to identify different groups of samples with similar properties, which could be linked to differences in process parameters and helped to identify physical mechanisms for the differences.

In this study, we investigated industrial HPMC-Si produced by REC Solar, both seeded and non-seeded. Although produced in 2014 and thus not representative of today's material quality, we believe the mechanisms described in this paper are general and are thus also valid for current production. The density of random angle grain boundaries, which is a good metric for the grain size, is influenced by the position in the ingot for non-seeded samples but not for seeded samples, and we therefore conclude it is related to differences in nucleation properties. There is a difference in the

coating morphology between the positions: the higher densities of random angle grain boundaries appear in the regions of rougher coating. On the other hand, the density of Σ3 and Σ27 boundaries was not influenced by the position but was similar for all the non-seeded samples, which was significantly higher than for the seeded samples. We link this to the probable dendritic growth mode during the initial growth phase due to a supercooling required for nucleation. The supercooling described for nucleation on silicon nitride is in the same range as that required for faceted dendritic growth.

Furthermore, we observe that the density of dislocation clusters correlates very well with the density of random angle grain boundaries and Σ27 boundaries, but not the density of Σ3 boundaries. The most striking correlation is between the ratio of densities of Σ27 and random angle grain boundaries, i.e., source/sink, measured in the bottom wafers and the density of dislocation clusters in the top wafers. From this we conclude that (1) the differences in dislocation density observed in these ingots are mainly related to the accumulation of differences in dislocation generation/annihilation by grain boundaries throughout the growth; (2) that these differences are set already at the very beginning through differences in nucleation/initial growth; and (3) that both the densities of source boundaries (e.g., Σ27) and sink boundaries (random angle boundaries) have direct and equal influences on the dislocation cluster density.

Thus, in order to further improve the quality of non-seeded high-performance multicrystalline silicon, it is necessary to focus on both these factors by adjusting different properties of the coating.

Author Contributions: Conceptualization, G.S., B.R. and A.S.; Methodology, G.S., A.S. and B.R.; Resources, A.S.; Investigation, G.S. and B.R.; Writing—Original Draft Preparation, G.S. and B.R.; Writing—Review & Editing, A.S.

Funding: This research was funded by the Norwegian Research Centre for Solar Cell Technology—Solar United and the Research Centre for Sustainable Solar Cell Technology—SuSolTech, which are supported by the Norwegian Research Council and industry partners.

Acknowledgments: The authors wish to thank the following people: Birgitte Karlsen (SINTEF) for sample preparation, Jorge Rituerto (SINTEF) for performing roughness measurements, Yang Pan (REC Solar) for sample selection and preparation.

Conflicts of Interest: REC Solar PTE. Ltd. Is one of several funding institutions of the research centres Solar United and SuSolTech. Adolphus Song of REC Solar PTE. Ltd. has participated in the reported work according to the author contribution described above.

References

1. Fraunhofer ISE: Photovoltaics Report. Available online: https://www.ise.fraunhofer.de/content/dam/ise/de/documents/publications/studies/Photovoltaics-Report.pdf (accessed on 10 August 2018).
2. Yang, Y.M.; Yu, A.; Hsu, B.; Hsu, W.C.; Yang, A.; Lan, C.W. Development of high-performance multicrystalline silicon for photovoltaic industry. *Prog. Photovolt. Res. Appl.* **2013**, *23*, 340–351. [CrossRef]
3. Lan, C.W.; Lan, A.; Yang, C.F.; Hsu, H.P.; Yang, M.; Yu, A.; Hsu, B.; Hsu, W.C.; Yang, A. The emergence of high-performance multi-crystalline silicon in photovoltaics. *J. Cryst. Growth* **2017**, *468*, 17–23. [CrossRef]
4. Ryningen, B.; Stokkan, G.; Kivambe, M.; Ervik, T.; Lohne, O. Growth of dislocation clusters during directional solidification of multicrystalline silicon ingots. *Acta Mater.* **2011**, *59*, 7703–7710. [CrossRef]
5. Stokkan, G. Relationship between dislocation density and nucleation in multicrystalline silicon. In Proceedings of the 6th International Symposium on Advanced Science and Technology of Silicon Materials, Kona, HI, USA, 19–23 November 2012; pp. 227–230.
6. Kohler, D.; Zuschlag, A.; Hahn, G. On the origin and formation of large defect clusters in multicrystalline silicon solar cells. *Sol. Energy Mater. Sol. Cells* **2014**, *120*, 275–281. [CrossRef]
7. Ervik, T.; Kivambe, M.; Stokkan, G.; Ryningen, B.; Lohne, O. Dislocation formation at ∑ = 27a boundaries in multicrystalline silicon for solar cells. In Proceedings of the 26th European Photovoltaic Solar Energy Conference and Exhibition, Hamburg, Germany, 5–9 September 2011; pp. 1895–1899.
8. Kohyama, M.; Yamamoto, R.; Doyama, M. Structures and energies of symmetrical 011 tilt grain boundaries in silicon. *Phys. Status Solidi B* **1986**, *137*, 11–20. [CrossRef]
9. Garg, A.; Clark, W.A.; Hirth, J.P. Dissociated and faceted large-angle coincident-site-lattice boundaries in silicon. *Philos. Mag. A* **1989**, *59*, 479–499. [CrossRef]

10. Garg, A.; Clark, W.A.; Hirth, J.P. Dislocation generation at near-coincidence site lattice grain boundaries during silicon directional solidification. *J. Cryst. Growth* **2015**, *411*, 12–18.
11. Stokkan, G.; Hu, Y.; Mjøs, Ø.; Juel, M. Study of evolution of dislocation clusters in high performance multicrystalline silicon. *Sol. Energy. Mater. Sol. Cells* **2014**, *130*, 679–685. [CrossRef]
12. Möller, H.J.; Funke, C.; Kreßner-Kiel, D.; Würzner, S. Growth optimization of multicrystalline silicon. *Engrgy Procedia* **2011**, *3*, 2–12. [CrossRef]
13. Ekstrøm, K.E.; Undheim, E.; Stokkan, G.; Arnberg, L.; Di Sabatino, M. Beta-Si_3N_4 particles as nucleation sites in multicrystalline silicon. *Acta Mater.* **2016**, *109*, 267–274. [CrossRef]
14. Sopori, B.L. A new defect etch for polycrystalline silicon. *J. Electrochem. Soc.* **1984**, *131*, 667–672. [CrossRef]
15. Sopori, B.; Wei, C.; Yi, Z.; Madjdpour, J. High-speed mapping of grown-in defects and their influence in large-area silicon photovoltaics. *J. Cryst. Growth* **2000**, *210*, 346–350. [CrossRef]
16. Stokkan, G. Characterisation of dislocation density of multicrystalline silicon wafers using the PVScan 6000. In Proceedings of the 22nd European Photovoltaic Solar Energy Conference, Milan, Italy, 3–7 September 2007; pp. 1282–1286.
17. Stokkan, G. Twinning in multicrystalline silicon for solar cells. *J. Cryst. Growth* **2013**, *384*, 107–113. [CrossRef]
18. Stokkan, G.; Stoss, A.; Kivambe, M.; Ervik, T.; Ryningen, B.; Lohne, O. Distribution of Grain Boundary Types in Multicrystalline Silicon. In Proceedings of the 28th European Photovoltaic Solar Energy Conference and Exhibition, Paris, France, 30 September–4 October 2013; pp. 1418–1421.
19. Ryningen, B.; Bellmann, M.; Kvande, R.; Lohne, O. The effect of crucible coating and the temperature field on minority carrier lifetime in directionally solidified multicrystalline silicon ingots. In Proceedings of the 27th European Photovoltaic Solar Energy Conference and Exhibition, Frankfurt, Germany, 24–28 September 2012.
20. Tsoutsouva, M.G.; Duffar, T.; Chaussende, D.; Kamguem, M. Undercooling measurement and nucleation study of silicon droplets on various substrates. *J. Cryst. Growth* **2016**, *451*, 103–112. [CrossRef]
21. Brynjulfsen, I.; Arnberg, L. Nucleation of silicon on Si_3N_4 coated SiO_2. *J. Cryst. Growth* **2011**, *331*, 64–67. [CrossRef]
22. Undheim, E.; Ekstrøm, K.E.; Arnberg, L.; Holmestad, R.; Di Sabatino, M. The effect of holding time on the size distribution of -Si_3N_4 particles and nucleation undercooling in multicrystalline silicon. *Phys. Status Solidi (C) Curr. Top. Phys.* **2016**, *13*, 822–826. [CrossRef]
23. Fujiwara, K.; Maeda, K.; Usami, N.; Sazaki, G.; Nose, Y.; Nomura, A.; Shishido, T.; Nakajima, K. In situ observation of Si faceted dendrite growth from low-degree-of-undercooling melts. *Acta Mater.* **2008**, *56*, 2663–2668. [CrossRef]
24. Undheim, E.; Maeda, K.; Arnberg, L.; Holmestad, R.; Fujiwara, K.; Di Sabatino, M. In-situ studies of multicrystalline silicon nucleation and growth on α-and β-Si_3N_4 coated substrates. *J. Cryst. Growth* **2018**, *482*, 75–84. [CrossRef]
25. Oriwol, D.; Trempa, M.; Sylla, L.; Leipner, H.S. Investigation of dislocation cluster evolution during directional solidification of multicrystalline silicon. *J. Cryst. Growth* **2017**, *463*, 1–9. [CrossRef]
26. Oriwol, D.; Carl, E.R.; Danilewsky, A.N.; Sylla, L.; Seifert, W.; Kittler, M.; Leipner, H.S. Small-angle subgrain boundaries emanating from dislocation pile-ups in multicrystalline silicon studied with synchrotron white-beam X-ray topography. *Acta Mater.* **2013**, *61*, 6903–6910. [CrossRef]
27. Lehmann, T.; Reimann, C.; Meissner, E.; Friedrich, J. Clarification of the relation between the grain structure of industrial grown mc-Si and the area fraction of electrical active defects by means of statistical grain structure evaluation. *Acta Mater.* **2016**, *106*, 98–105. [CrossRef]
28. Trempa, M.; Kupka, I.; Kranert, C.; Lehmann, T.; Reimann, C.; Friedrich, J. Evolution of grain structure and recombination active dislocations in extraordinary tall conventional and high performance multi-crystalline silicon ingots. *J. Cryst. Growth* **2017**, *459*, 67–75. [CrossRef]

© 2018 by the authors. Licensee MDPI, Basel, Switzerland. This article is an open access article distributed under the terms and conditions of the Creative Commons Attribution (CC BY) license (http://creativecommons.org/licenses/by/4.0/).